Abnormal hopping conduction in semiconducting polycrystalline graphene

Jeongho Park,[1,*] William C. Mitchel,[1] Said Elhamri,[2] Larry Grazulis,[1] and Igor Altfeder[1]

[1]*Air Force Research Laboratory, Materials and Manufacturing Directorate (AFRL/RXAN) Wright-Patterson AFB, Ohio 45433-7707, USA*

[2]*Departments of Physics, University of Dayton, Dayton, Ohio 45469, USA*

(Received 19 September 2012; revised manuscript received 17 April 2013; published 11 July 2013)

We report the observation of an abnormal carrier transport phenomenon in polycrystalline semiconducting graphene grown by solid carbon source molecular beam epitaxy. At the lowest temperatures in samples with small grain size, the conduction does not obey the two-dimensional Mott-type variable-range hopping (VRH) conduction often reported in semiconducting graphene. The hopping exponent p is found to deviate from the 1/3 value expected for Mott VRH with several samples exhibiting a $p = 2/5$ dependence. We also show that the maximum energy difference between hopping sites is larger than the activation energy for nearest-neighbor hopping, violating the assumptions of the Mott model. The 2/5 dependence more closely agrees with the quasi-one-dimensional VRH model proposed by Fogler, Teber, and Shklovskii (FTS). In the FTS model, conduction occurs by tunneling between neighboring metallic wires. We suggest that metallic edge states and conductive grain boundaries play the role of the metallic wires in the FTS model.

DOI: 10.1103/PhysRevB.88.035419 PACS number(s): 72.20.Ee, 72.80.Vp

The extraordinary properties of graphene have driven research on novel electronic devices and large-area growth on a variety of substrates. Among the challenges, the development of a better understanding of the transport properties in both semimetallic and semiconducting graphene is crucial to enable practical application of this novel material. Since growth techniques such as chemical vapor deposition on metal films and foils result in polycrystalline material, an understanding of the role of edge states and grain boundaries is critical. To that end, significant experimental and theoretical effort has been put into understanding the characteristics of edge states and grain boundaries in graphene. The electronic properties of edge states strongly depend on their atomic configuration. Ritter and Lyding[1] observed that a zigzag edge has a higher conductance than an armchair one due to the localized states associated with the zigzag edge. Grain boundaries are formed by the coalescence of misoriented graphene grains with edges consisting of various atomic configurations (zigzag, armchair, and a combination of these). The coalescence of two misoriented graphene grains forms a one-dimensional (1D) topological defect at the grain boundary. Recently, Lahiri *et al.*[2] suggested that a line of repeating pentagon-heptagon defects generates electron states near the graphene Fermi energy and that the defects showed characteristics of conducting metallic wires. These unique electronic structure properties might alter the charge distribution over the graphene layer and affect the overall carrier transport in macroscopic graphene films. In addition, another topic of current interest is hopping conduction in semiconducting graphene that can dominate the low-temperature conduction process. Three conduction mechanisms have been used to explain the temperature dependence of the resistivity of semiconducting graphene: thermal activation, nearest-neighbor hopping (NNH) conduction, and variable-range hopping (VRH) conduction, where the conduction follows the relation[3–5] $R(T) \propto \exp(T_0/T)^p$. The specifics of VRH are described by the hopping exponent p and the characteristic temperature T_0. Mott VRH with $p = 1/3$ is often used to explain low-temperature resistivity,[4,6,7] but a $p = 1/2$, suggestive of Efros-Shklovskii (ES) VRH,[8] which includes Coulomb interactions, has also been reported.[5] ES VRH has also been found in a two-dimensional (2D) array of quantum dots formed from reduced graphene oxide.[9] However, as we show here, the low-temperature conduction in polycrystalline semiconductor graphene is abnormal in that it does not always follow either Mott or ES VRH. In the samples studied here, the temperature dependence more closely follows that predicted for the quasi-1D VRH model of Fogler, Teber, and Shklovskii (FTS).[10] We suggest that this quasi-1D hopping behavior might originate from the hopping conduction between grain boundaries/edge states that show metallic conduction.

The samples studied were all grown on chemical mechanically polished, on-axis semi-insulating Si-face 6H-SiC substrates by carbon molecular beam epitaxy (CMBE) using the graphite filament (GF) heater as the carbon source as well as the heater,[11] which produces polycrystalline graphene. For comparison, crystalline graphene was grown by CMBE using a C_{60} carbon source. Large-area van der Pauw samples for temperature-dependent resistivity and Hall effect measurements were made by depositing indium contacts directly on the corners of 1-cm $\times$ 1-cm square samples without any other processing. Electrical measurements, Raman spectroscopy, scanning tunneling microscopy (STM), and conductive atomic force microscopy (CAFM) were all made on the same samples. Gating was not employed, so we were unable to vary the carrier concentration with an external electric field.

Figure 1 shows the typical surface morphology of the graphene grown by the GF source. The STM image clearly shows that the graphene layer consists of small grains with boundaries between the coalesced grains. Since there will be no STM signal from the semi-insulating SiC, it is assumed that the graphene film is continuous. The roughly straight steps are due to the small off-cut angle of the SiC substrate. In this image hexagonal grains that have yet to coalesce into a second layer are visible. The height difference between the first layer and the grains is 3.2 nm, as expected for a single layer of graphene. The grain size ranges from several to tens of nanometers. These typically have a hexagonal shape with 120° corners. Interestingly, individual grains in Fig. 1 are often

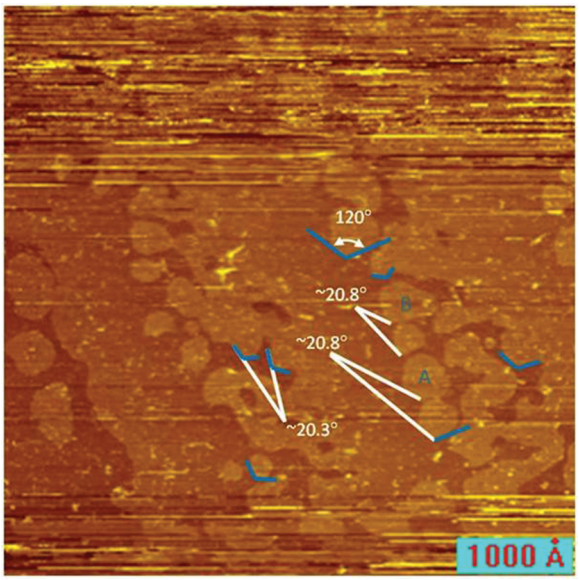

FIG. 1. (Color online) STM image of polycrystalline graphene grown by solid source CMBE. STM images were obtained at 30-mV bias and 0.9 nA under an ultrahigh vacuum environment. The atomic steps and the grains have 0.32-nm thickness, indicating monolayer graphene.

misaligned with each other by approximately 20°. When a misaligned grain merges with another, a tilt grain boundary forms at the edge between the grains. The orientations of the coalesced grains (A and B in Fig. 1) typically differ by 20.8°. This mismatch might produce periodically distributed point defects at the grain boundary.[12] Lahiri *et al.*[2] reported that this type of extended defect acts as a quasi-1D metallic wire, which might become a possible conduction path.

To understand the conduction properties in polycrystalline graphene, the temperature-dependent resistivity $R(T)$ and Hall effect were measured as shown in Fig. 2 for a typical polycrystalline sample. At high temperatures, both the resistivity and carrier concentration n show activated behavior with similar temperature dependences, which is typical of semiconducting graphene.[3–6] The rapid increase in carrier density and quick drop in resistivity with increasing temperature for $T > 140$ K [solid red color region in Figs. 2(a) and 2(b)] are due to thermal activation of carriers. The origin of the band gap in this material is discussed in a previous report.[13] At lower temperatures R and n deviate from activated behavior, and the rate of increase in R with decreasing T is reduced. As seen in Fig. 2(b), the distinguishing feature of concentration data is the deviation from thermal activation and increase in the scatter in the data for the low-temperature region even though the resistivity data remain clean to the lowest temperatures. The observation of the scatter in the carrier concentration suggests that hopping is the dominant conduction mechanism in this temperature region since hopping carriers are not expected to show a Hall effect. Zou and Zhu[4] explained a similar T dependence of the resistivity of graphene at the charge neutrality point (CNP) as the combination of three different conduction mechanisms, such as thermal activation, NNH, and 2D Mott's VRH ($p = 1/3$). According to our resistivity and carrier density measurements, we can also

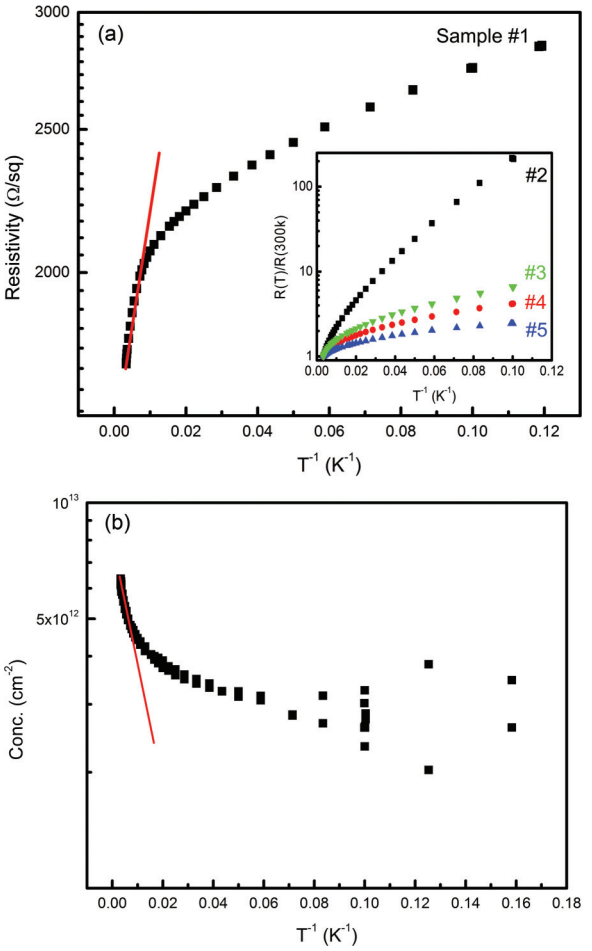

FIG. 2. (Color online) Temperature-dependent transport measurements. (a) Resistivity vs inverse temperature. The solid red color line indicates the region of thermal activation. Insert: Normalized temperature-dependent carrier conduction of five polycrystalline samples. (b) The corresponding temperature-dependent carrier density. At low temperature, the scattered data indicates the presence of hopping conduction.

attribute the low-temperature data to a combination of NNH and VRH. The conduction in the intermediate-temperature region is dominated by NNH, while that at low temperature is dominated by VRH. The inset in Fig. 2(a) shows R vs $1000/T$ for the other polycrystalline samples in this study. We attempted to fit the data with the model proposed by Zou and Zhu.[4] However, the use of $p = 1/3$ for VRH resulted in an unphysical negative resistivity for the NNH component (Appendix A, Table III). The model proposed by Zou and Zhu[4] describes the low-temperature conduction at the CNP as a hopping process between the charge fluctuations associated with electron and hole puddles,[4] which resulted in the relation $R_{NP}(T) \propto \exp(T_0/T)^{1/3}$. However, the samples studied here are not at the CNP. To address the low-temperature hopping conduction behavior, we adapted the dimensionless activation method developed by Zabrodskii *et al.*[14] in order to ensure a relative high accuracy in the determination of the functional form of the T-dependent resistivity as well as the related parameters for VRH conduction, even though the variation in the resistivity over the temperature range VRH that is dominant

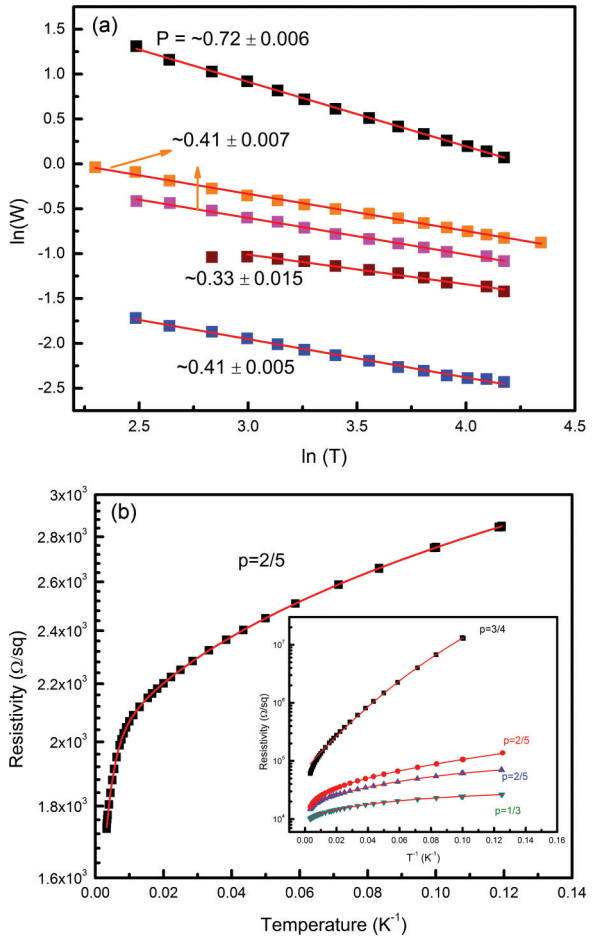

FIG. 3. (Color online) (a) Determination of hopping exponent p for all five polycrystalline samples from the slope of $\log W$ vs p $\log T$ plot using the relation $\ln W = -p \ln T + constant$. (b) Fitting results for resistivity of a representative polycrystalline sample using p value determined above ($p = 2/5$). Insert: Fitting results for remaining samples showing good agreement with FTS models of VRH.

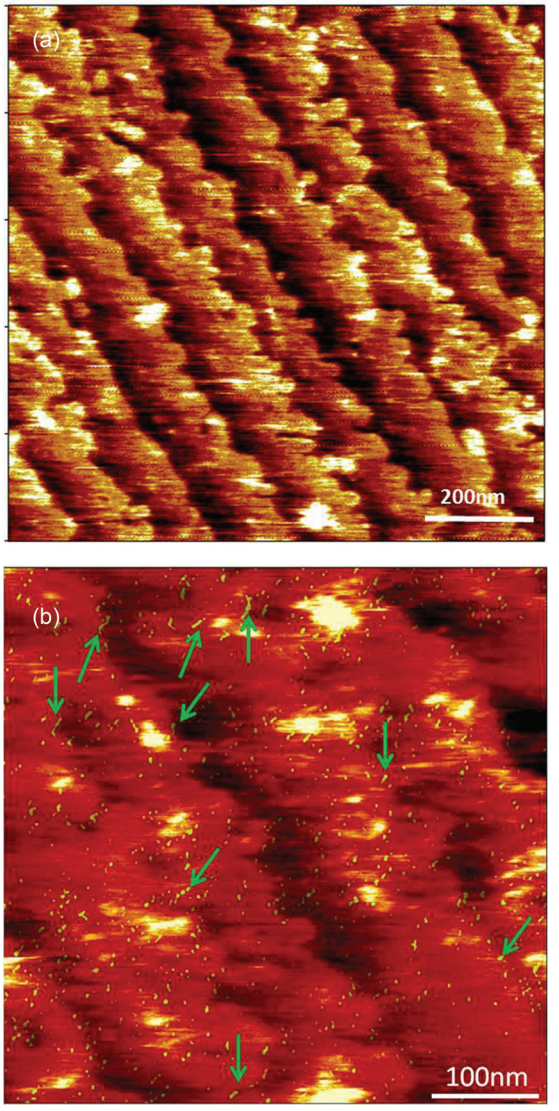

FIG. 4. (Color online) (a) Surface morphology taken by CAFM, 1 mm × 1 mm. (b) Overlay of the current map on the surface morphology image. Green-colored arrows point to the high-current edges.

is small. Zabrodiskii defined a reduced activation energy of the conductivity ($w \equiv \frac{\varepsilon}{kT} = \frac{T^{-1}\partial \ln \rho}{\partial T^{-1}}$). The general form of the resistivity in the VRH region is

$$\rho(T) = BT^{-m} \exp(T_0/T)^p, \tag{1}$$

where B, m, T_0, and p are constants. The reduced activation energy w can thus be expressed by

$$w(T) = m + x(T_0/T)^p. \tag{2}$$

Since the second term is much larger than that of the first term (m), we have

$$\ln(w(T)) \approx \ln(x(T_0)^p) - p\ln(T), \tag{3}$$

where $\ln(x(T_0)^p)$ is constant. By plotting $\ln(w)$ vs $\ln(T)$, we could directly obtain the hopping exponent p in Eq. (1). Figure 3(a) shows the linear region of $\ln(w)$ vs $\ln(T)$ plots for the samples in this study. Three different values of p were obtained from the five samples, $p = 0.33$ (1/3), 0.41 (2/5), and 0.72 (3/4). The value $p = 1/3$ was obtained from the crystalline graphene grown with the C_{60} source. The other two values ($p = 2/4$ and 3/4) were obtained from the polycrystalline graphene samples grown by GF CMBE. As seen in Fig. 3(b), fits of the resistivity to a sum of thermal activation, NNH, and VRH with p fixed to the values determined above are very good. Comparisons of the goodness of fit for each data set with each of the three values of p are provided in Appendix B. Interestingly, the values obtained for the polycrystalline graphene, $p = 0.41$ (2/5) and 0.72 (3/4), all deviated from the Mott VRH value of 1/3, which was only observed in the crystalline C_{60}-grown sample. This deviation explains why the fitting results with Mott VRH (Zho and Zhu model) did not explain our resistivity data. We will discuss the possible origin later.

The polycrystalline graphene consists of many grains and grain boundaries. Since there have been reports of enhanced conduction at edges and grain boundaries[1,2] the current distribution over the polycrystalline surface might

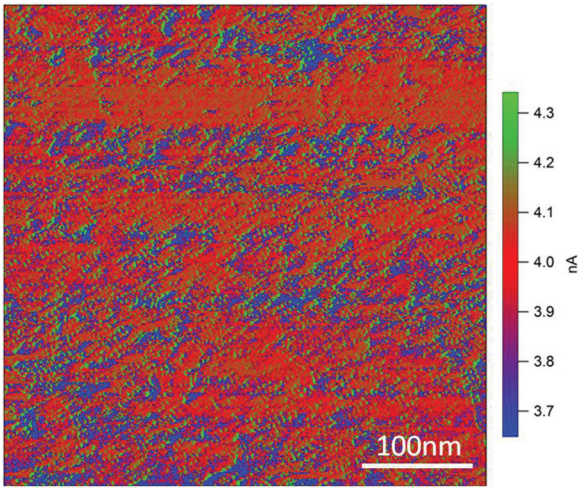

FIG. 5. (Color online) The current map of the polycrystalline graphene was measured by conductive AFM. It shows relatively uniform current flow over the surface, indicating that the graphene continuously covers the surface.

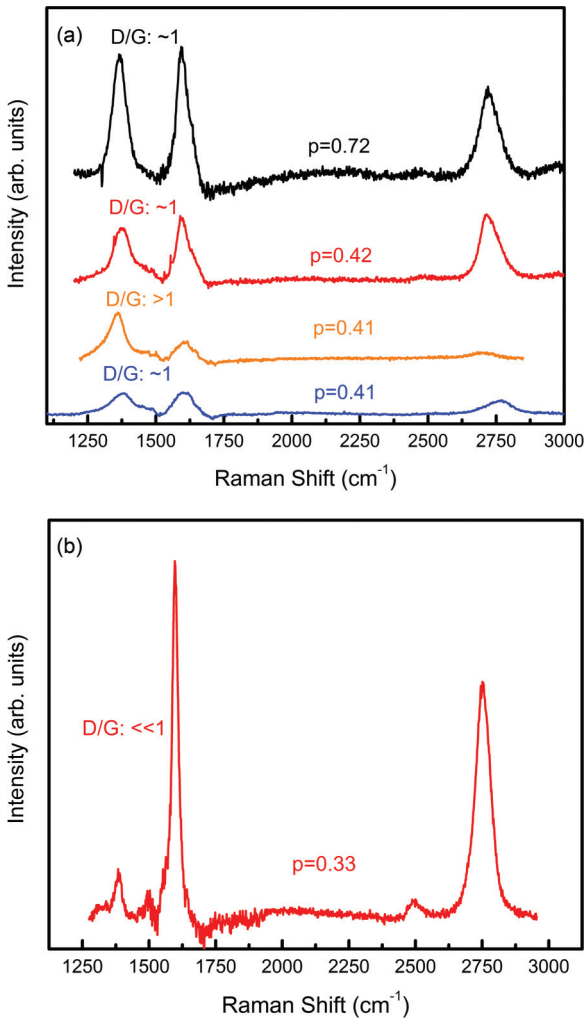

FIG. 6. (Color online) (a) Raman spectra of polycrystalline graphene samples grown from GF carbon source. (b) Raman spectra of sample grown from C_{60} carbon source. This sample shows Mott VRH.

be inhomogeneous if these edges or grain boundaries are associated with high conductance. Figure 4(a) shows that surface morphology taken by AFM is very similar to the STM image (Fig. 1), which also shows tens of nanometer-size isolated grains as well as merged grains. As will be shown in Fig. 5, the current map from the CAFM measurement showed continuous current over the surface, which suggests a continuous graphene layer on the semi-insulating SiC surface. We did observed an inhomogeneous current distribution in the CAFM image with the higher values tending to follow a rough network of lines. To show the relation between higher current regions and the corresponding morphology, we overlaid the current map on the morphology image in Fig. 4(b). Close examination of Fig. 4(b) shows that the localized high current (green arrows) is located at both the step edges and on the steps themselves. Comparing with the STM results shown in Fig. 1, these high-current regions on the steps may possibly result from grain boundaries.[2] In addition, the high-current regions at the boundaries and edges could be associated with the different atomic configuration of the edge state.[1] These conductive edges/boundaries may possibly contribute to the charge transport over the polycrystalline graphene, if the carrier density inside the grains is smaller than that of edges/boundaries, in which case they would act as a network of conducting wires.

In Fig. 6(a) we show the results of Raman spectroscopy measurements on the polycrystalline samples for which the hopping exponent p deviated from the Mott VRH value of $1/3$ and the crystalline graphene sample ($p = 1/3$). As can be seen, the intensity of the D band is comparable to or bigger than that of the G band in these samples. By using the relation[15] between the D/G ratio and the grain size of graphitic materials, the average grain size of our polycrystalline graphene can be estimated at tens of nanometers, which agrees well with the estimated grain size from the STM image in Fig. 1. The small grain size in these samples will lead to a high density of grain boundaries and edge states and also a reduced distance between neighboring edges/boundaries, which might increase the possibility of hopping through them. Figure 6(b) shows the Raman spectrum for a sample grown using the C_{60} carbon source,[11] which had a VRH exponent of $1/3$. Note that this is not the polycrystalline sample with $p = 1/3$ in Fig. 2. The D/G ratio of this sample is a least ten times smaller than those of the polycrystalline samples, suggesting that grain size is at least ten times bigger than that of the samples deviated from Mott's hopping conduction. The larger grain size should reduce the density of boundaries.

Here, we discuss the possible origin for the deviation from the Mott VRH in our polycrystalline graphene. The Mott model for VRH was developed for doped crystalline semiconductors and amorphous materials, so it is not immediately obvious that it is appropriate for graphene. The appropriateness of this model can be tested by exploring the assumptions inherent in the model. In the Mott regime, the VRH activation energy ε is a function of temperature and varies as $T^{2/3}$. In NNH

TABLE I. Validity check of 2D Mott VRH conduction ($p = 1/3$) in polycrystalline graphene as discussed in the text. All samples show that $\varepsilon_{\max}$ is wider than E_N, suggesting disagreement with Mott law at the low temperatures.

Samples	Experimental p	NNH	2D Mott's VRH	$e_{\max}$ (meV)	E_N (meV)
No. 1	0.41	77 K–35 K	<26 K	2.24	1.62
No. 2	0.33	77 K–30 K	<23 K	1.6	1.1
No. 3	0.41	77 K–26 K	<17 K	3.85	1.92
No. 4	0.72	77 K–26 K	<23 K	16.3	5.1
No. 5	0.42	77 K–35 K	<30 K	0.99	0.4

conduction, the activation does not vary with temperature, and average hopping distance is the mean separation between impurities. In Mott VRH, the maximum energy ($\varepsilon_{\max}$) difference between localized states should be less than impurity band width ($\Delta\varepsilon$) near Fermi energy. At the critical temperature (T_c) at which the Mott hopping occurs, we can obtain the relation below[8]

$$\varepsilon_{\max} = k\left(T_o T_c^2\right)^{1/3}, \tag{4}$$

where T_0 is the characteristic temperature of Mott VRH conduction and k is Boltzmann constant. When density of states (DOS) of localized states abruptly vanishes at a certain distance from the Fermi energy, we obtain that activation energy of NNH (E_N) equal to 5/6 $\Delta\varepsilon$.

$$\Delta\varepsilon \approx \tfrac{6}{5} E_N. \tag{5}$$

Therefore, the use of Mott VRH is valid if the relation below satisfies[8]

$$\varepsilon_{\max} = k\left(T_o T_c^2\right)^{1/3} \leqslant \tfrac{6}{5} E_N = \Delta\varepsilon. \tag{6}$$

By fitting the data in the intermediate-temperature range with NNH conduction $\rho = \rho_N e^{(E_N/k_B T)}$, we obtained the value of $E_N = 1.92$ meV. The critical temperature of VRH conduction was obtained from the highest temperature for which a linear dependence in ln ρ vs $T^{-1/3}$ was found. As will be shown in Fig. 8 (Appendix C), the critical temperature was ~17 K. The characteristic temperature T_0 was obtained by fitting the resistivity data below 17 K with the Mott's conduction ($\rho = \rho_N e^{(\frac{T_0}{T})^{1/3}}$), yielding the value of $T_0 = \sim 320$ K. By putting all these experimental values into Eqs. (4) and (5), we find $\varepsilon_{\max} \approx 3.89$ meV, which is two times wider than $E_N \approx 1.92$ meV. This violates the important assumption of Mott VRH [Eq. (6)] and suggests that that model might not be appropriate for these samples. Table I summarizes the validity check of 2D Mott VRH for the five polycrystalline samples and experimental p values obtained from the reduced activation method (RAM). The temperature range for NNH and 2D Mott VRH was estimated by taking the linear regions of the ln ρ vs T^{-1} and ln ρ vs $T^{-1/3}$ plots, respectively. All samples show that $\varepsilon_{\max}$ is wider than E_N, indicating that the Mott VRH model is not valid in these polycrystalline samples. The sample showing the lower D/G ratio [Fig. 6(b)] had $\varepsilon_{\max} =$ ~0.15 meV and $\Delta\varepsilon =$ ~1.73 meV, which agrees with the Mott assumption and supports the assignment of $p = 1/3$ for that sample to Mott VRH.

The p values we obtained are consistent with the quasi-1D VRH conduction model recently proposed by FTS.[10] In the FTS model, the electrons are tightly localized in a Wigner crystal. The impurities pin this electron crystal and divide the crystal into segments, which behave as individual metallic rods. The conduction occurs due to electrons tunneling between neighboring rods. According to the FTS model, the hopping exponent p can be expressed[10] by

$$p = \frac{\mu + 1}{\mu + d + 1}, \tag{7}$$

where d is the dimensionality of the array of the 1D rods and μ is the exponent of a power-law-dependent DOS ($g(\varepsilon) \sim |\varepsilon|^{\mu}$, $\mu = 0, 1,$ or 2). Table II shows the summarized tunneling dimension d and μ values corresponding to the observed p values. In the case of $p = 2/5$, the DOS near the Fermi energy, $g(\varepsilon)$, is of the form $|\varepsilon|$, representing a linear Coulomb gap due to metallic screening of the Coulomb potential.[10] For $p = 3/4$, the FTS model suggests a parabolic Coulomb gap near the Fermi energy, whose DOS has the form $|\varepsilon|^2$. With the conventional percolation method, one can estimate[16] the size of the Coulomb gap, $\Delta \approx k(\frac{1}{2})(T_0^3 T_v)^{\frac{1}{4}}$, where k is the Boltzmann constant, T_0 is the VRH characteristic temperature, and T_v is the VRH onset temperature. T_v is determined by the

TABLE II. Predicted hopping conduction exponent p vs possible electron tunneling dimension, d, and energy exponent of the DOS $g(\epsilon) \propto \varepsilon^{\mu}$.

Hopping exponent (p)	Tunneling dimension	A power law of DOS $g(\epsilon) \propto \varepsilon^{\mu}$
2/5	3D	$\mu = 1$
1/3	2D	0
3/4	1D	2

TABLE III. (Color online) The comparison of the fitting results between $p = 1/3$ and $p = 2/5$ in hopping exponent terms for the sample in Fig. 2(a).

	$p = 1/3$ (Mott hopping)		$p = 2/5$ (RAM)	
	Value	Standard error	Value	Standard error
$1/\rho_{ac}$	2.576 97E-4	4.390 83E-6	2.732 05E-4	3.413 42E-6
$\varepsilon_{\mathbf{a}}$	37.802 22	0.7062	36.593 71	0.516 11
$1/\rho_{\mathrm{NNH}}$	−2.690 49E-5	9.275 14E-7	3.595 29E-5	4.646 56E-6
E_n	5.571 93	0.3885	0.919 34	0.084 77
$1/\rho_{\mathrm{VRH}}$	6.455 03E-4	2.096 11E-6	5.250 18E-4	7.486 16E-6
T_0	1.890 74	0.031 65	1.024 74	0.080 18

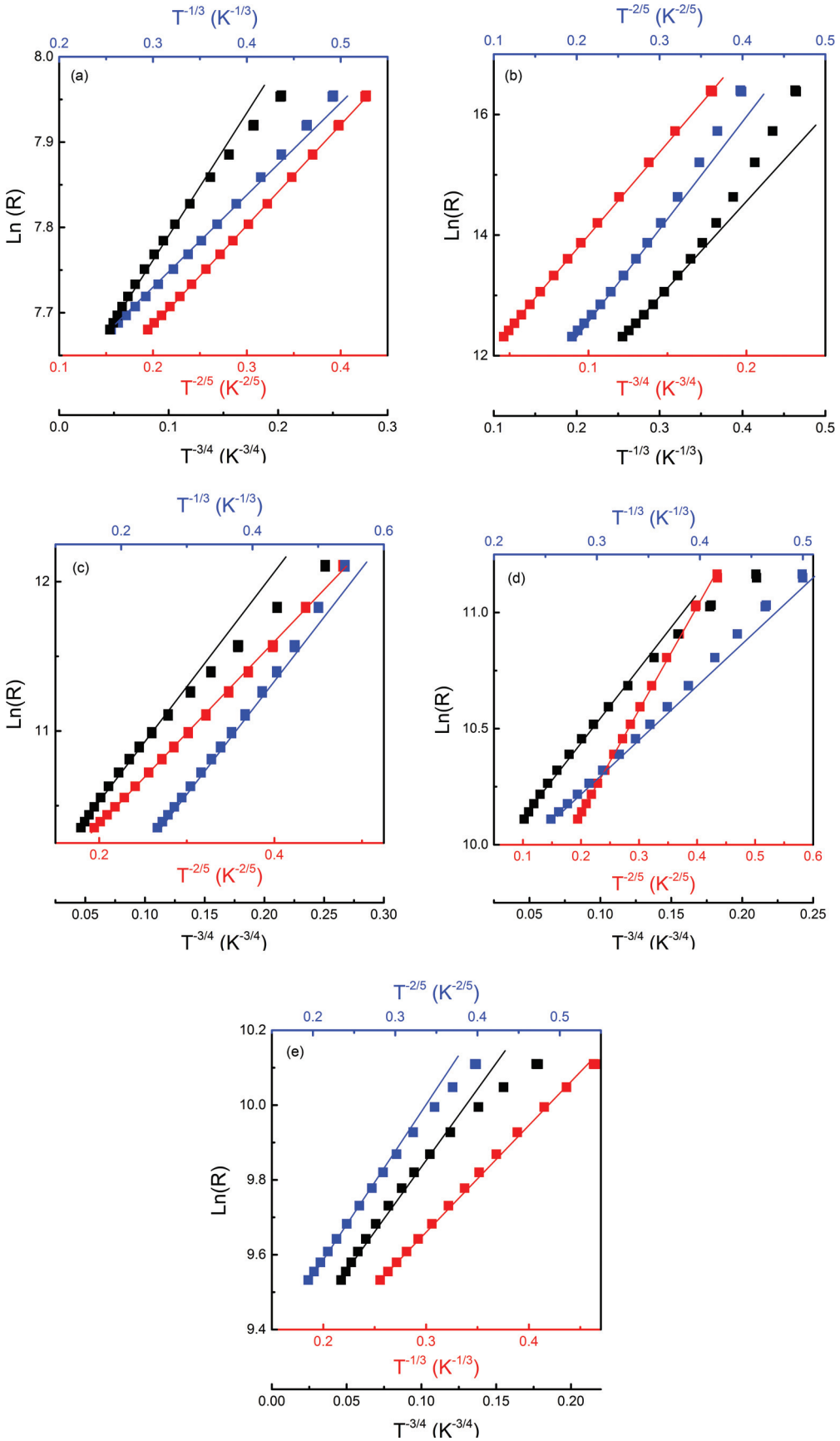

FIG. 7. (Color online) Plots of ln (R) vs $(1/T)^p$ of the data shown in Fig. 2 for three different values of p ($p = 1/3, 3/4, 2/5$). The straight lines are guides to the eye. The red color data and axis corresponds to the p value obtained from the RAM. Plots (a)–(e) correspond to samples numbers 1–5 in Fig. 2(a), respectively.

transition temperature between NNH and VRH. By fitting the temperature-dependent resistivity data [Fig. 3(b)], we find that T_0, E_n, and T_v are ~92 K, ~5.1 meV, and ~20 K respectively. The estimated Coulomb gap Δ is ~2.7 meV and is less than the NNH activation energy E_n, which is a requirement of the FTS model. Another requirement for this model is that the dimensionless parameter $r_s \equiv \frac{a}{2a_B}$, where a is the average distance between electrons along the chain direction and a_B is the effective Bohr radius that exceeds unity. The VRH characteristic temperature for $p = 3/4$ is expressed[10] as

$$T_0 = C_2 \frac{e^2}{\kappa l}\left[\frac{a_\perp^2\sqrt{r_s}}{\xi_\perp^2}\ln\left(\frac{l}{a_\perp}\right)\right]^{1/3}, \tag{8}$$

where κ is the dielectric constant, $a_\perp^2$ is the area per chain, r_s is a dimensionless parameter, $\xi_\perp$ is the transverse localization length, and C_2 is numerical factor of the order of unity. By using the definition of $\xi_\perp$ in the Ref. 10 we obtain the relation $kT_0 \sim E_N r_s^{1/6}$, yielding $r_s \sim 14$. Therefore, the two conditions $\Delta < E_n$ and $r_s > 1$ for the FTS model are met in our polycrystalline graphene.

At high temperatures, the conduction is mainly due to thermal activation to the bands, but as the temperature decreases, the thermally activated carriers start to decrease, and NNH takes over, the polycrystalline graphene becomes insulating due to lack of thermally activated carriers and carriers originating from the high-current regions [Fig. 4(b)] might be dominant, and these would contribute to macroscopic low-temperature conduction through hopping between wires. Therefore, the quasi-1D VRH conduction model (FTS model) well explains low-temperature conduction behavior and leads to the assumption that the main conduction mechanism of this polycrystalline graphene at low temperature is hopping between a network of 1D conducting wires made up of grain boundaries or edge states as observed in Fig. 4(b).

In conclusion, we have found deviations from Mott VRH in the low-temperature conductivity of polycrystalline graphene grown by solid source CMBE. The deviations correlate with grain size as determined from the ratio of the intensities of the Raman D and G bands with stronger deviations for the smaller grain size. The data are explained in terms of the quasi-ID VRH model of FTS.[10] Conductive AFM measurements suggest that the grain boundaries or edge states in isolated grains play the part of the conducting wires in the FTS model.

ACKNOWLEDGMENTS

This work was supported by the Air Force office of Scientific Research (Harold Weinstock). We thank G. Landis for technical assistance.

APPENDIX A: THE FITTING OF T-DEPENDENT RESISTIVITY WITH MOTT VRH

Temperature-dependent conduction in semiconductor materials can be described by

$$\rho = \rho_{ac} e^{-\frac{\varepsilon_a}{kT}} + \rho_{\mathrm{NNH}} e^{-\frac{E_n}{kT}} + \rho_{\mathrm{VRH}} e^{-(\frac{T_0}{T})^p}, \tag{A1}$$

where ε_a is the thermal activation energy for band-gap transitions, ε_n is the NNH activation energy, T_0 is the characteristic temperature of VRH conduction, and p is the hopping exponent that depends on the DOS near Fermi energy. Tailored graphene such as gated samples (gapped) shows 2D Mott VRH for which the hopping exponent $p = 1/3$. Temperature-dependent resistivity data from Fig. 2(a) were fitted with the above three conduction mechanisms with VRH exponents $p = 2/5$, which were obtained from the RAM, and $p = 1/3$ for conventional Mott VRH, while the other parameters were determined from the fit. The best fit results are shown in Table III. The Mott hopping exponent ($p = 1/3$) resulted in negative values for the NNH resistivity terms. However, the exponent $p = 2/5$ resulted in good fits with positive values for the resistivity and activation energy terms for samples, where RAM indicated this exponent. This suggests that conduction models, including Mott VRH, do not explain the low T conduction in this sample.

APPENDIX B: THE VALIDITY CHECK OF THE HOPPING EXPONENTS

In the VRH temperature region, the ln (R) vs $(1/T)^p$ plots should have a linear relationship when the hopping

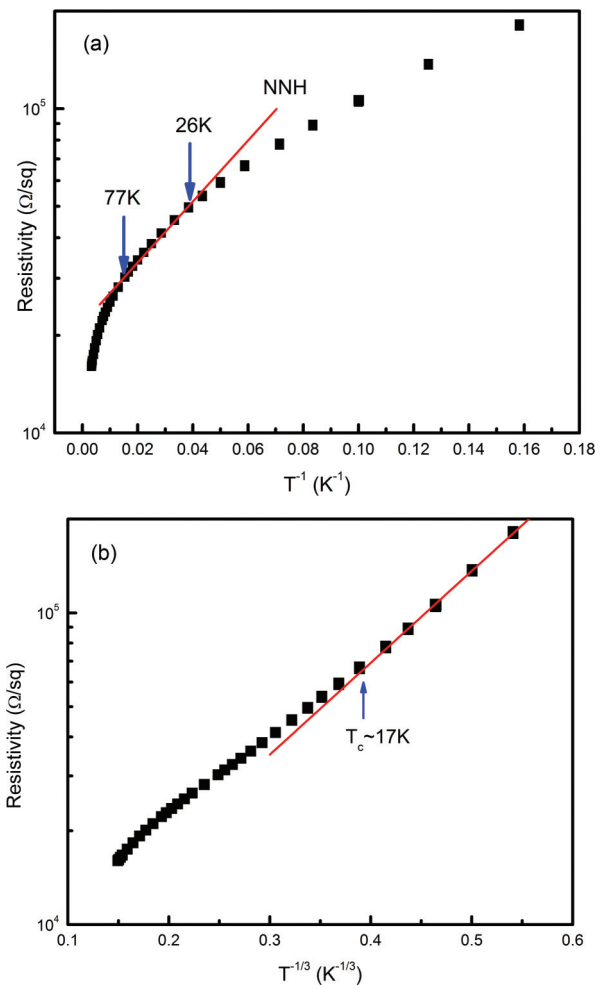

FIG. 8. (Color online) The plots of (a) ln ρ vs T^{-1} and (b) ln ρ vs $T^{-1/3}$.

exponent p is correct. Therefore, this relation can be used for a validity check of the obtained hopping exponents. The temperature-dependent resistivity data for each sample shown in Fig. 2 are plotted in Fig. 7 as ln (R) vs $(1/T)^p$ with three different p values ($p = 1/3$, $3/4$, $2/5$). As seen, each data set has a linear relation with only one hopping exponent, and that is the value that resulted from the RAM. The fitting results in the paper over the entire temperature range and these validity checks, therefore, suggest that our hopping exponents well explain the hopping conduction in GF graphene.

APPENDIX C: NNH TEMPERATURE RANGE AND THE CRITICAL TEMPERATURE TO CHECK VALIDITY OF 2D MOTT VRH

To obtain the temperature range for NNH and the critical temperature for 2D Mott VRH, the resistivity data are plotted as ln ρ vs T^{-1} and ln ρ vs $T^{-1/3}$ in Figs. 8(a) and 8(b), respectively. The linear region in plot of ln ρ vs T^{-1} was used to determine the NNH temperature range, while the critical temperature (T_C) of the 2D Mott VRH conduction was also obtained from the linear region of ln ρ vs $T^{-1/3}$ plot at the lower-temperature region.

*Author to whom correspondence should be addressed: jeongho.park@wpafb.af.mil

[1]K. A. Ritter and J. W. Lyding, Nat. Mater. **8**, 235 (2009).
[2]J. Lahiri, Y. Lin, P. Bozkurt, I. I. Oleynik, and M. Batzill, Nat. Nanotechnol. **5**, 326 (2010).
[3]J. B. Oostinga, H. B. Heersche, X. L. Liu, A. F. Morpurgo, and L. M. K. Vandersypen, Nat. Mater. **7**, 151 (2008).
[4]K. Zou and J. Zhu, Phys. Rev. B **82**, 081407 (2010).
[5]M. Y. Han, J. C. Brant, and P. Kim, Phys. Rev. Lett. **104**, 056801 (2010).
[6]J. Yan and M. S. Fuhrer, Nano Lett. **10**, 4521 (2010).
[7]A. B. Kaiser, C. Gómez-Navarro, R. S. Sundaram, M. Burghard, and K. Kern, Nano Lett. **9**, 1787 (2009).
[8]B. I. Shklovskii and A. L. Efros, *Electronic Properties of Doped Semiconductors* (Springer-Verlag, Berlin, 1984).
[9]D. Joung, L. Zhai, and S. I. Khondaker, Phys. Rev. B **83**, 115323 (2011).
[10]M. M. Fogler, S. Teber, and B. I. Shklovskii, Phys. Rev. B **69**, 035413 (2004).
[11]J. H. Park, W. C. Mitchel, L. Grazulis, H. E. Smith, K. G. Eyink, J. J. Boeckl, D. H. Tomich, S. D. Pacley, and J. E. Hoelscher, Adv. Mater. **22**, 4140 (2010).
[12]J. Cervenka and C. F. J. Flipse, Phys. Rev. B **79**, 195429 (2009).
[13]J. H. Park, W. C. Mitchel, S. Elhamri, and T. C. Back, Appl. Phys. Lett. **100**, 133107 (2012).
[14]A. G. Zabrodskii, Sov. Phys. Semicond. **11** 345 (1977).
[15]L. G. Cancado, K. Takai, T. Enoki, M. Endo, H. Mizusaki, A. Jorio, R. Magalhaes-Paniago, and M. A. Pimenta, Appl. Phys. Lett. **88**, 163106 (2006).
[16]K. G. Lisunov, N. Wizent, A. Waske, J. Werner, N. Tristan, C. Sekar, G. Krabbes, G. Behr, E. Arushanov, and B. Büchner, J. Appl. Phys. **103**, 123712 (2008).